Molecular Cell, Volume *56*

Supplemental Information

Structural Model of Active Bax at the Membrane

Stephanie Bleicken, Gunnar Jeschke, Carolin Stegmueller, Raquel Salvador-Gallego, Ana J. García-Sáez, and Enrica Bordignon

Supplemental Figures

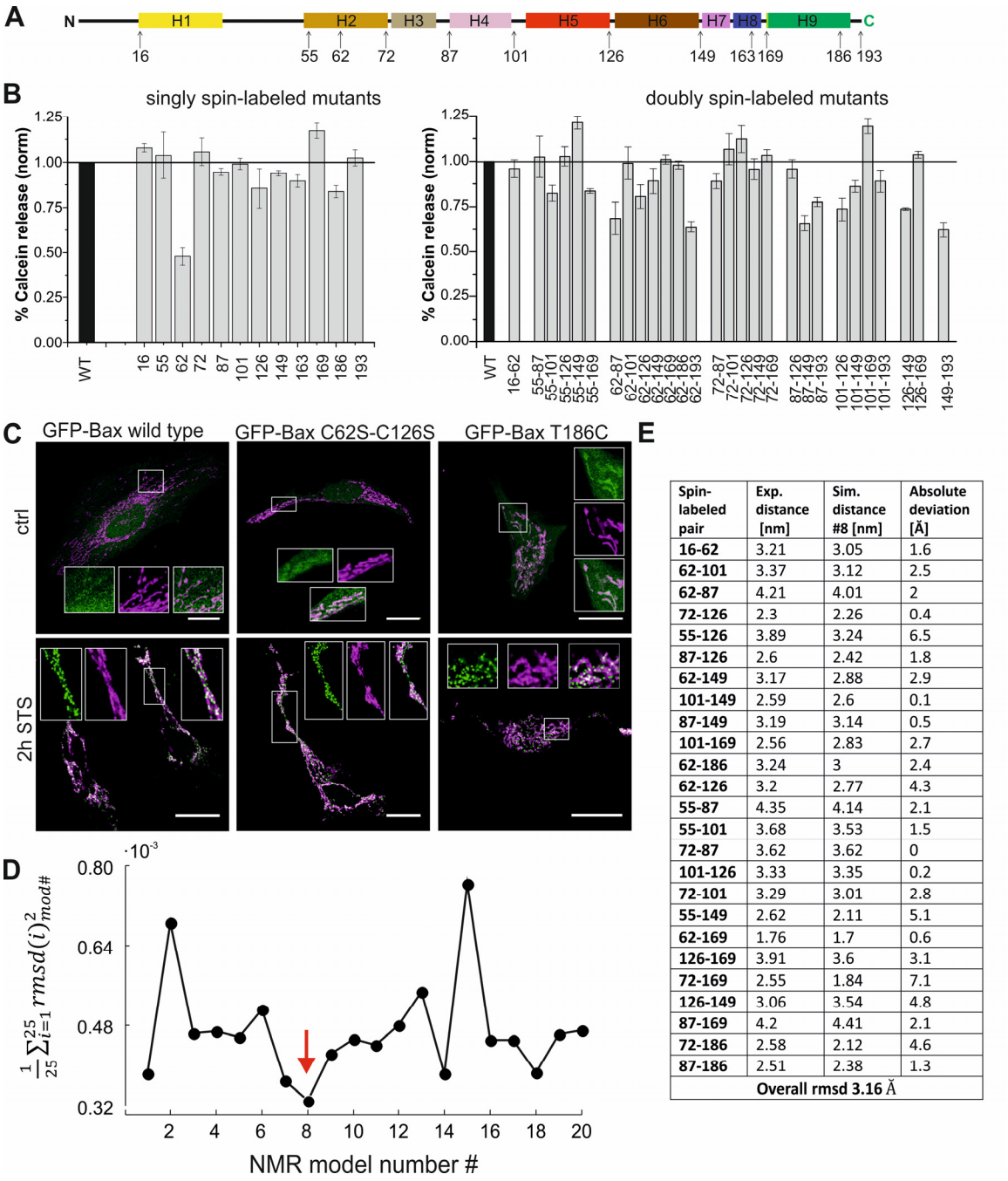

E

Spin-labeled pair	Exp. distance [nm]	Sim. distance #8 [nm]	Absolute deviation [Å]
16-62	3.21	3.05	1.6
62-101	3.37	3.12	2.5
62-87	4.21	4.01	2
72-126	2.3	2.26	0.4
55-126	3.89	3.24	6.5
87-126	2.6	2.42	1.8
62-149	3.17	2.88	2.9
101-149	2.59	2.6	0.1
87-149	3.19	3.14	0.5
101-169	2.56	2.83	2.7
62-186	3.24	3	2.4
62-126	3.2	2.77	4.3
55-87	4.35	4.14	2.1
55-101	3.68	3.53	1.5
72-87	3.62	3.62	0
101-126	3.33	3.35	0.2
72-101	3.29	3.01	2.8
55-149	2.62	2.11	5.1
62-169	1.76	1.7	0.6
126-169	3.91	3.6	3.1
72-169	2.55	1.84	7.1
126-149	3.06	3.54	4.8
87-169	4.2	4.41	2.1
72-186	2.58	2.12	4.6
87-186	2.51	2.38	1.3
Overall rmsd 3.16 Å			

Figure S1. Quality control of the investigated Bax mutants. Related to Figure 1. (A) Scheme of the secondary structure of Bax with all labeled sites highlighted. (B) Membrane

permeabilization assay of spin-labeled Bax mutants compared to Bax WT. The release of calcein from LUVs in the presence of 100 nM Bax and 20 nM cBid was measured after 2 h incubation at RT (labeled site/s indicated under the grey bars) and normalized to Bax WT (black bar). Shown are the mean and the SEM (n=6). In this case, the confidence interval ($CI_{95\%}$) is ±2.477·SEM. As an example the $CI_{95\%}$ for the mutant 62R1 is [0.36, 0.60], and for 55R1-149R1 is [1.12, 1.30]. (C) Fixed HeLa cells co-transfected with Mito-DsRed2 (magenta) and GFP-Bax (green; wild type or mutant as indicated in the figure) under control conditions or after 2 h incubation with 1 µM staurosporin. Scale bar: 20 µm. Inset show zoom in pictures of the different channels. (D) Square deviations between experimental DEER time traces obtained for the 25 doubly labeled mutants and the traces simulated for each NMR model (mod. #) (*rmsd* is the root mean square deviation). The comparison shows that most NMR models represent well spin-labeled monomeric Bax in buffer solution. The best scored model is #8 (arrow). (E) Comparison of interspin distances within monomeric, inactive Bax measured experimentally and simulated on the NMR model #8 (PDB 1F16).

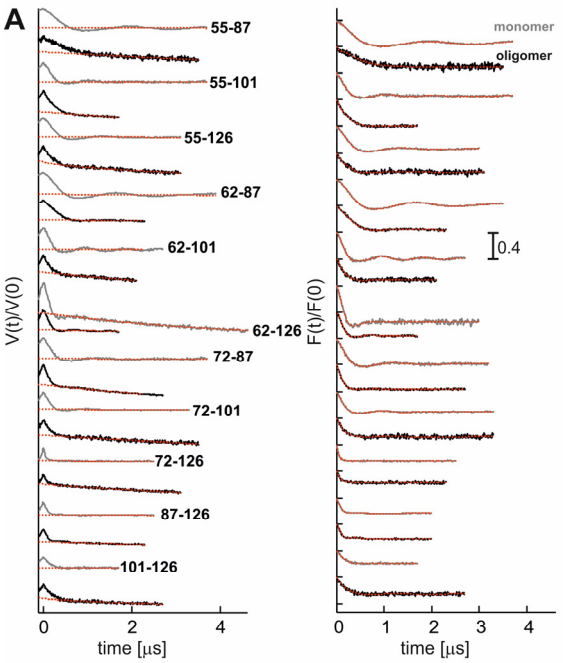

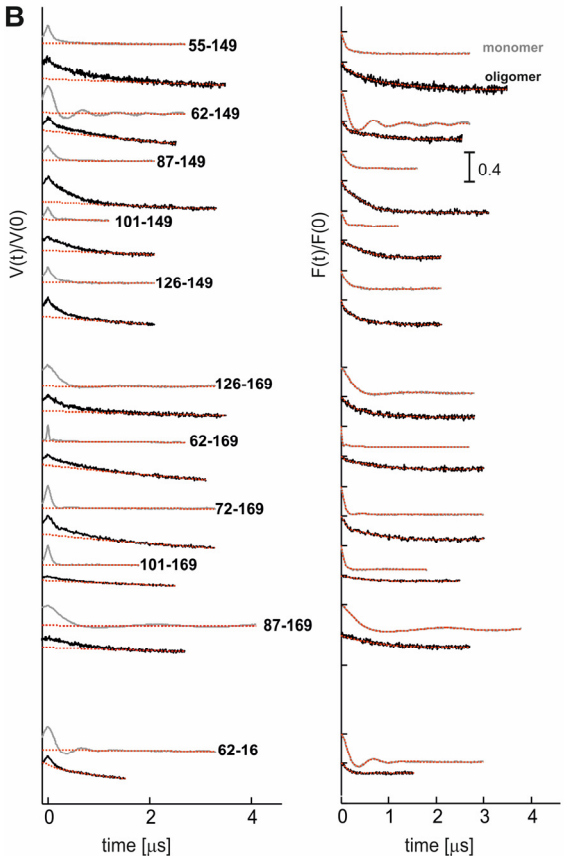

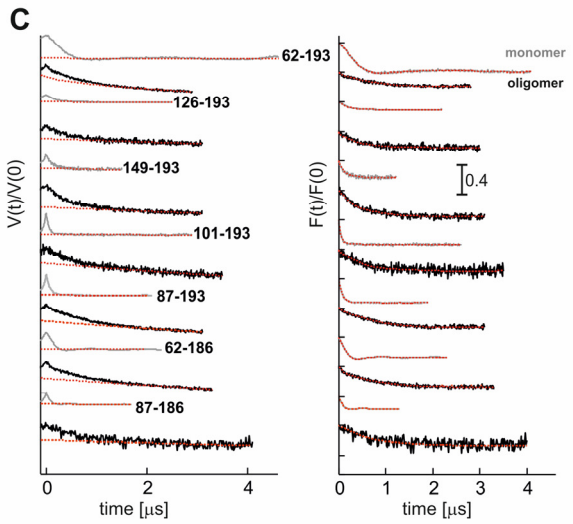

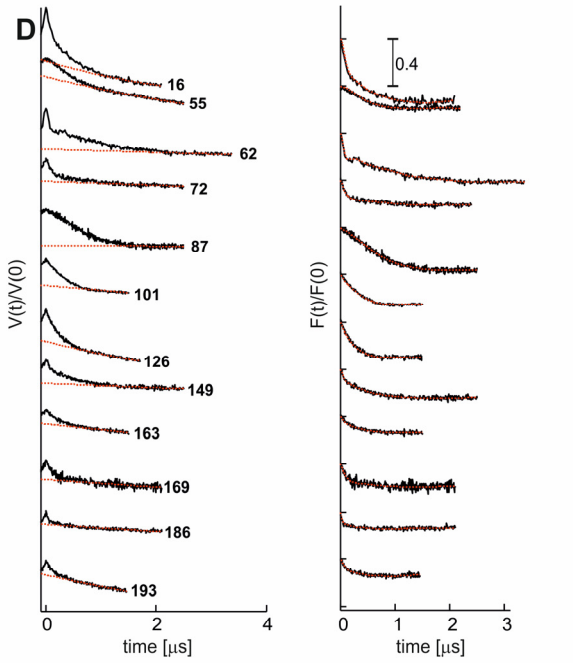

E

Spin-labeled pair	Exp. distance [nm]	Sim. distance [nm]	Absolute deviation [Å]	Spin-labeled pair	Exp. distance [nm]	Sim. distance [nm]	Absolute deviation [Å]
55-55	4.8	4.82	0.2	**72-126**	2.28	1.95	3.3
62-62	2.32	2.44	1.2	**55-126**	3.83	4.04	2.1
72-72	2.92	2.72	2	**55-87**	4.93	5.25	3.2
87-87	5.31	5.27	0.4	**55-101**	3.54	4.52	9.8
101-101	4.26	4.93	6.7	**72-87**	2.98	3.36	3.8
126-126	3.57	3.77	2	**101-126**	3.71	3.38	3.3
62-87	4.16	4.34	1.8	**62-101**	3.27	3.71	4.4
87-126	2.67	2.14	5.3	**72-101**	3.11	3.57	4.6
62-126	3.14	3.17	0.3	**Overall rmsd 4.01 Å**			

Figure S2. Primary DEER data and fits. Related to Figures 1-3. (A-D) Left, experimental Q-band DEER primary data V(t)/V(0) and simulated background function (red, dotted line, 3D homogeneous background). Right, DEER traces after background correction and fit with DeerAnalysis2013 (red, dotted line) with Tikhonov regularization parameters from 10 to 1000 adjusted to the type of trace obtained experimentally (e.g. via L-curve analysis and data validation, data not shown). The vertical bar shows the 0.4 tick mark, which helps to analyze the modulation depths in the F(t)/F(0) data. Color code: monomeric Bax in water (grey) and membrane-embedded, oligomeric Bax (black). (A) Pairs within the *dimerization* domain; (B) pairs connecting the *dimerization* domain to positions 149 and 169; (C) pairs connecting the *dimerization* domain to probes in helix 9; (D) singly labeled mutants in the membrane-embedded state. (E) Comparison of interspin distances within membrane-embedded oligomeric Bax measured experimentally and simulated on the X-ray structure of the truncated Bax dimer (PBD:4BDU (Czabotar et al., 2013)) elongated up to residue 126.

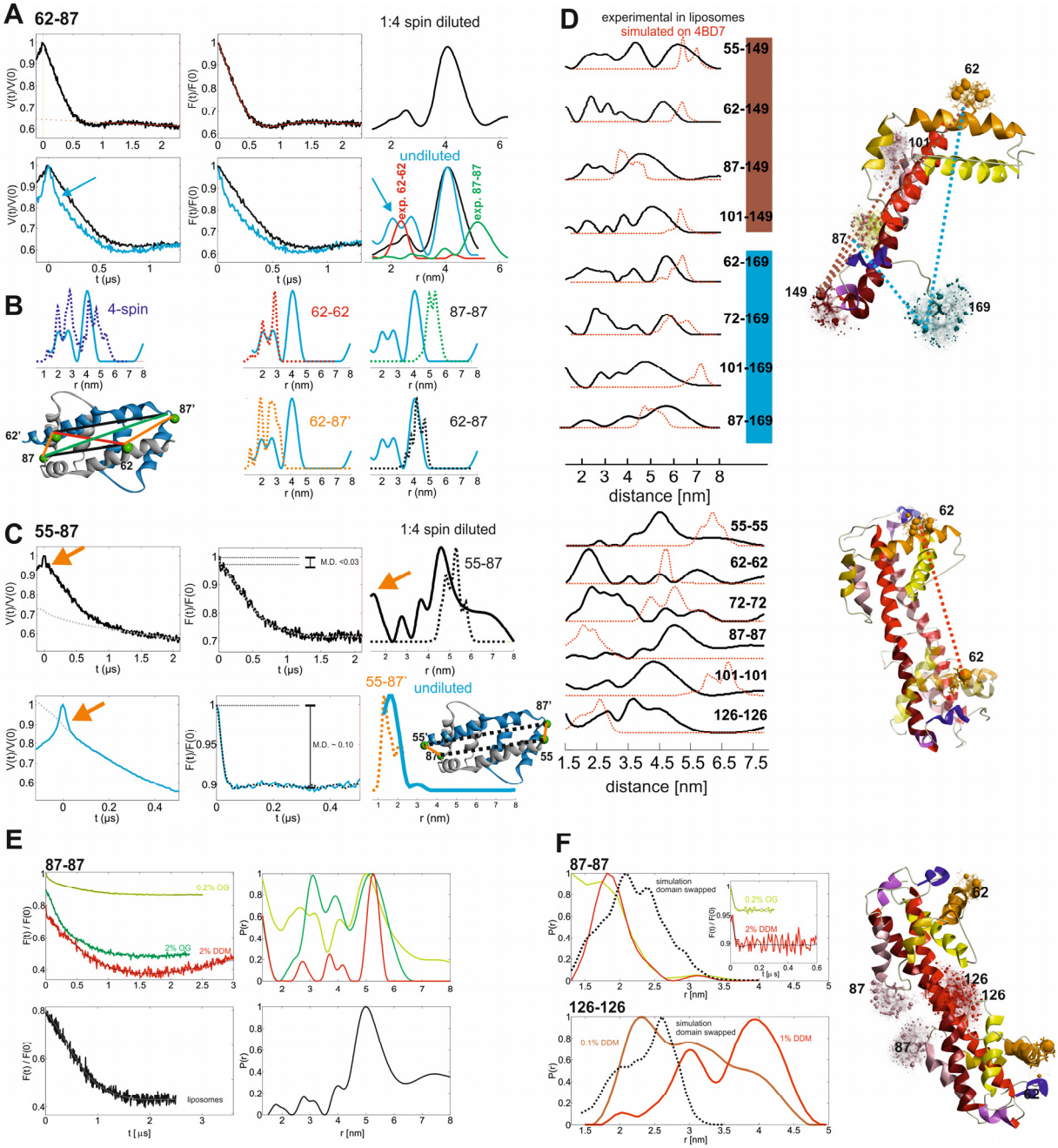

Figure S3. Validation of the spin dilution method and correlation between Bax domain-swapped dimer and experimental data. Related to Figure 2. (A) Upper panels: DEER analysis of the spin-diluted sample (1:4, black). Lower panels: DEER analysis of the undiluted sample

(cyan). The spin-diluted sample allows to retrieve the 4 nm peak, which is in agreement with simulated 62-87 distances in the crystallized dimerization domain (see Figure 3). The undiluted sample instead shows an increased fraction of short distances due to monomer-monomer interactions. Superimposed in black are the experimental traces and distances of the spin diluted sample. In the distance distribution panel, the experimental 62-62 distance is shown in red and the experimental 87-87 distance in green (the long distances 87-87 are not detected in the too short DEER trace of the undiluted sample). (B) Upper left panel: All possible distance distributions on the four-spin system of a Bax dimer labeled at residues 62 and 87 (dotted blue line), as simulated with MMM2013.2 on the dimeric X-ray structure 4BTU (shown in the lower left panel). No ghost peaks (Jeschke et al., 2009; von Hagens et al., 2013) are observed. Right panels: Simulated contributions of each spin pair (different colors, dotted lines) compared to the undiluted distances distribution (cyan). (C) Effect of spin dilution on Bax doubly labeled at residues 55 and 87. Upper panels: The DEER analysis on the spin-diluted sample reveals a main component at 4.5 nm (in agreement with the 55-87 simulated distance on the X-ray structure 4BDU, dotted black upper panel) together with a barely detectable fraction of short distances in the trace (modulation depth < 0.03, orange arrow). Lower panels: A short DEER trace detected in the undiluted sample (cyan, lower panels) shows an increased modulation depth (up to 0.1) for this component (orange arrow), which represent the 55-87' inter-monomeric distance in the dimer (simulated distance in dotted orange). The short 55-87' distance is in line with cross-linking observed in Bax in the closely related 55-94 positions (Dewson et al., 2012) and our own cross linking data (Figure 5A). (D) Left panels: Experimental distances from doubly and singly labeled, membrane-embedded Bax (black) compared to distances simulated on the domain-swapped dimer (dotted red). Right panels: Schematic view of one monomer or both monomers of the domain swapped dimer (X-ray structure

4BD7 (Czabotar et al., 2013)) with some simulated spin-labeled rotamers highlighted. The distance comparison demonstrates that the experimental data in the membrane are incompatible with the domain swapped dimer, as the inter-monomer distances are very different. (E) Effect of different detergent concentrations (depicted in the panels) on the DEER distances detected on Bax singly labeled at position 87. Short distances appear at low detergent concentration, which are absent in liposomes and only marginally populated at 2% w/v DDM. The distance centered at around 5 nm obtained in liposomes and DDM shows that the two environments favor the same confirmation of Bax in the dimerization domain (previously proven for 62 and 126 as well in (Bleicken et al., 2010)). (F) Analysis of two short DEER traces at 0.2% w/v OG and 2% w/v DDM shows that the short 87-87 distances are similar to those simulated for the domain-swapped dimer (black dotted, see structure on the right). Previously at low DDM concentration also the two labels at position 126 showed distances in the 2 nm range (Bleicken et al., 2010), also similar to those simulated in the domain-swapped dimer. The X-ray structure of the domain-swapped dimer with spin labels attached at positions 62 (as a reference in the BH3 domains), 87 and 126 is shown on the right.

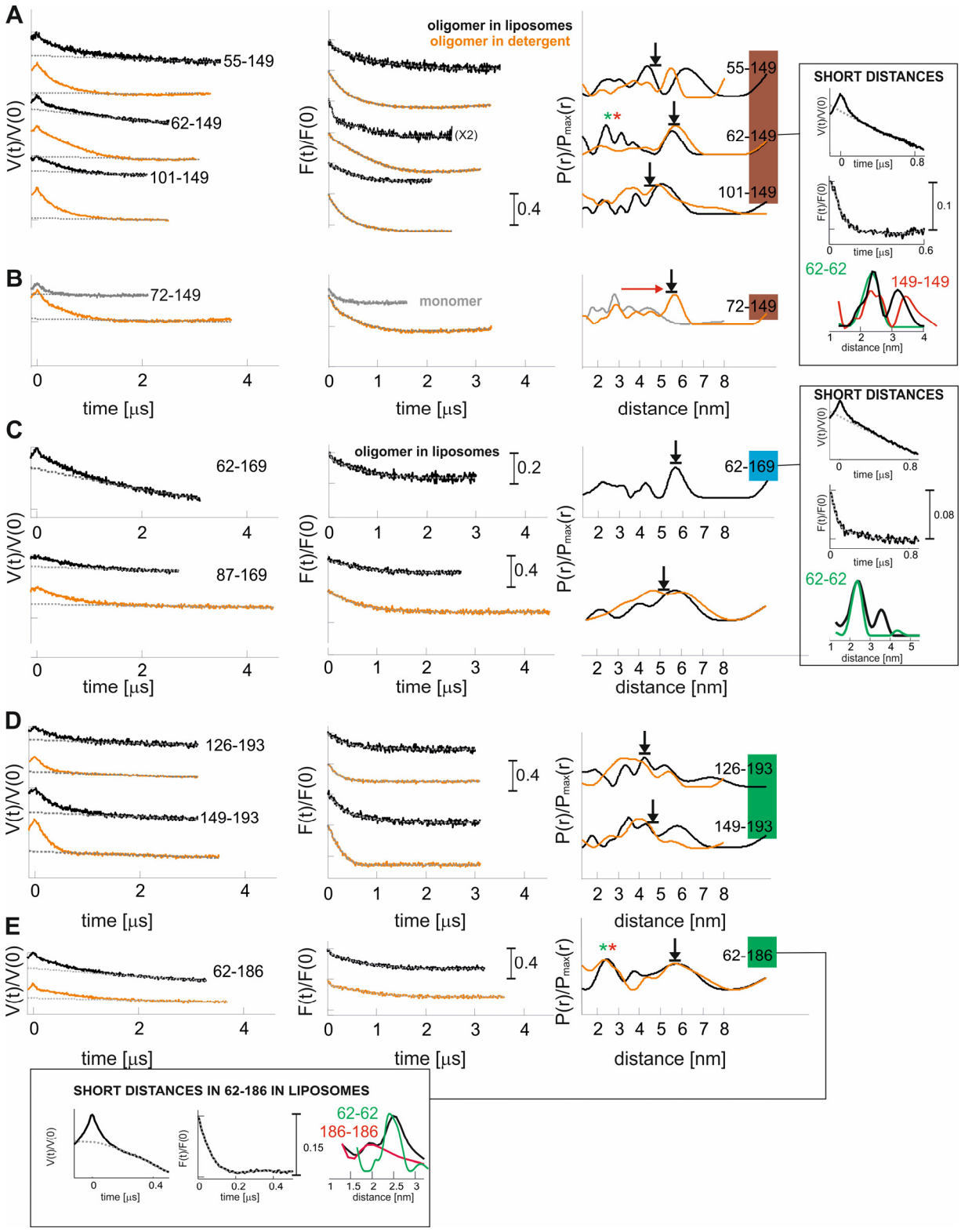
A
55-149
62-149
101-149
V(t)/V(0)
oligomer in liposomes
oligomer in detergent
(X2)
0.4
F(t)/F(0)
P(r)/Pmax(r)
**
SHORT DISTANCES
0.1
62-62
149-149
distance [nm]
B
72-149
monomer
time [µs]
distance [nm]
C
62-169
87-169
oligomer in liposomes
0.2
0.4
0.08
D
126-193
149-193
E
62-186
SHORT DISTANCES IN 62-186 IN LIPOSOMES
0.15
62-62
186-186

Figure S4. Validation of peak assignment between *dimerization* and *piercing* domains. Related to Figure 2. (A) Detergent (2% w/v DDM) and liposome DEER data on three pairs, in which one label is within the *dimerization* domain and the other one at residue 149 in the *piercing* domain. For 62-149, the peak assignment was relatively straightforward as the residual 62-62 (green asterisk) and 149-149 (red asterisk) distances, are clearly shorter than the intra-monomeric 62-149 distance (black arrow) present in liposomes and in detergent. To further prove that the short distances are due to the residual distances after spin dilution, the inset in the box shows an 800 ns DEER trace and the resulting distance distribution (black) superimposed to the 62-62 (green) and 149-149 (red) experimental distances. The agreement confirms the assignment of the long distance to the 62-149 intra-monomeric constraint. For 55-149, the peak assignment is more difficult because the 55-55 distance is already in the 5 nm range. The samples in detergent and in LUVs (see black and orange lines in 55-149) show some deviation, therefore we used an average distance for the modeling approach (black arrow). For 101-149 both samples in detergent and in LUVs (see black and orange lines in 101-149) show broad distance distribution. The constraint chosen is indicated by the black arrow. (B) The 72-149 pair is shown in the monomeric inactive water soluble Bax (grey) and in detergent (orange). Due to the poor labeling efficiency of this mutant, only traces in detergent were detected. The constraint chosen is indicated by the black arrow. (C) The short distance in the distribution of the pair 62-169 in LUVs is assigned to the intra-dimer 62-62 distance. The peak at 5.7 nm is assigned to the intra-monomeric distance (black arrow). The inset in the box shows a short DEER trace analyzed to extract only the short distance peak, and the comparison with the 62-62 distance distribution. The same analysis done on the 72-169 site pair confirmed that the peak at 2.5 nm is in agreement with the 72-72 distance as well (data not shown). The broad distance between 87 and 169 is confirmed both in liposomes and detergent. (D-

E) The distances to the C-terminal helix 9 (positions 193 and 186) are broadly distributed both in liposomes and detergent. The intra-monomeric main distances used to build the isosurfaces for position 193 and 186 are visualized with the black arrows. The inset in the box shows a 400 ns DEER trace analyzed using as background the region from 100 to 400 ns to highlight that for 62-186 the short distances < 3 nm agree very well with the 62-62 and 186-186 distances (red and green asterisks), which are not perfectly suppressed by spin dilution.

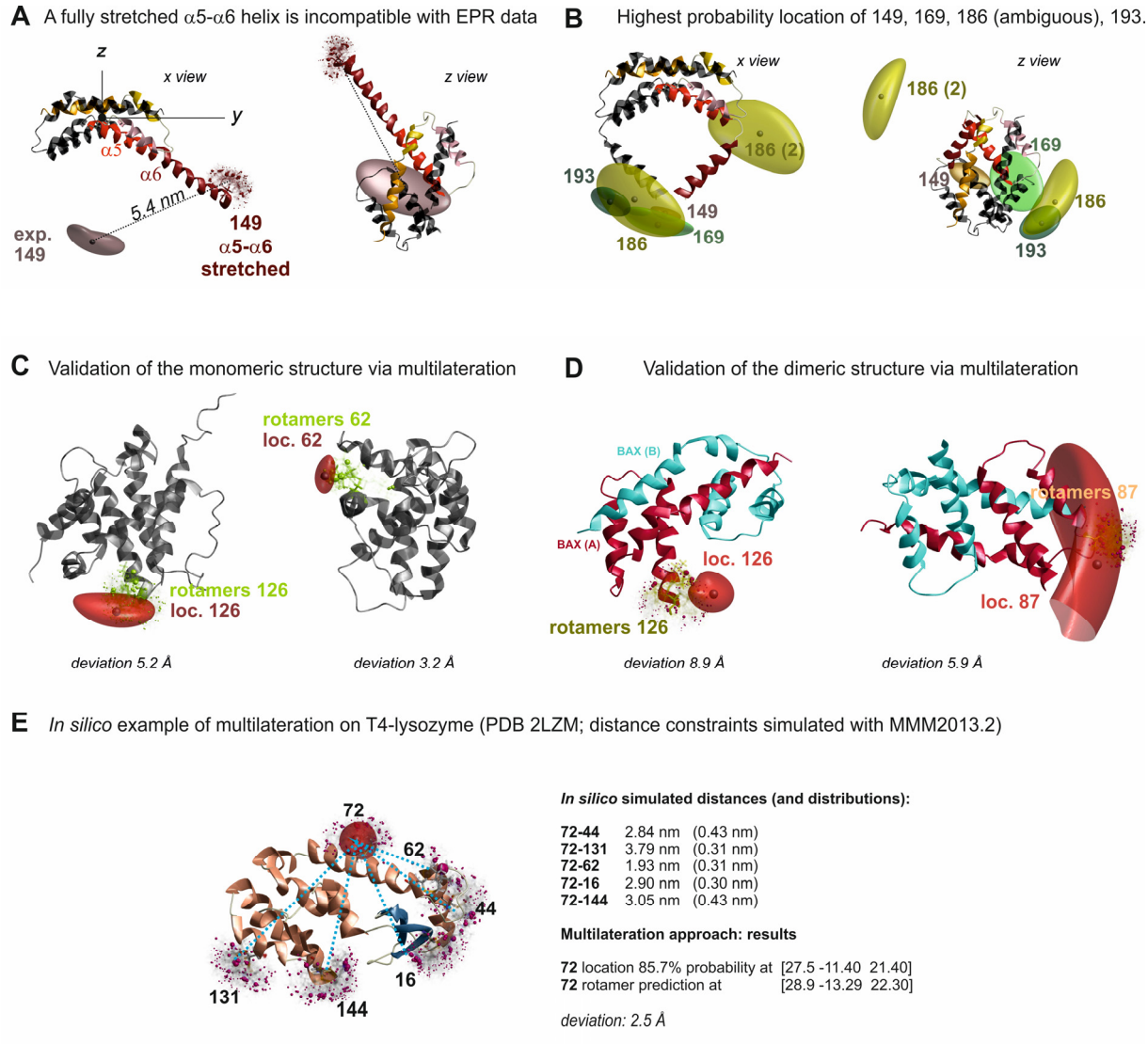

Figure S5. Additional information on the modeling approach. Related to Figure 4. (A) Two orthogonal views of the dimerization domain of Bax with helix 5 elongated *in silico* as one fully stretched helix up to the spin-labeled residue 149 (chain A: colored, chain B: dark grey). The localization of 149 used for the structural model proposed (brown isosurface) is presented, which deviates by > 5 nm from the expected position of a stretched helix 5/6. (B) Two orthogonal views of the most probable model of membrane-embedded dimers (helices 2-6, see Figures 4A, B) together with the three isosurfaces for the localization of the spin labels at position 169 (light

green), 186 (yellow) and 193 (dark green) created using the constraints from the doubly labeled Bax mutants. The location of 186 is ambiguous due to a small number of constraints available, therefore two isosurfaces are presented. Only the one close to the modeled 169 and 193 is compatible with the other data. (C) Insights into the validation of the multilateration process, using experimental distances obtained in monomeric Bax for position 126 and 62 (model #8 PDB: 1F16). The calculated isosurfaces are superimposed to the simulated rotamers in the NMR model #8 (more details in the supplementary methods). (D) Insights into the validation of the multilateration process, using experimental distances obtained in membrane-embedded Bax for position 126 and 87 (dimeric structure 4BDU elongated up to residue 126). More details are given in the supplemental methods. (E) *In silico* example of the multilateration approach performed with MMM2013.2 on the 1.7 Ă resolution structure of T4-lysozyme (PDB 2LZM). The MTSL rotamers calculated on the six positions are shown as stick representation. The spheres centered at the midpoint of the N-O bond represent the probability of the rotamer. We calculated the localization of the spin-labeled site at position 72 (in transparent red the probability density isosurface including 50% of the total probability for finding the spin label) based on *in silico* simulated distances to the 5 sites labeled with MMM2013.2 (distances and width of the distribution presented on the right inset). The highest probability of location of 72 (with the x, y, z coordinates given in parenthesis on the right inset) deviates only 2.5 Ă from the mean N-O-midpoint of the simulated rotamers at the same site.

Supplemental methods (SM)

Supplemental methods: Experimental procedures

Protein production and spin labeling

All Bax mutants were cloned using site directed mutagenesis followed by DNA sequencing. Full length mouse Bid, and full length human Bax were expressed in *E. coli.* All Bax mutants were purified as described in (Bleicken et al., 2010). From Bid, cBid was cleaved and purified as described in (Bleicken et al., 2010; Desagher et al., 1999). Cysteine 193 was chemically attached to the Bax protein using the intein cleavage reaction as described in (Chong et al., 1997). The MTSL spin label (1-Oxyl-2,2,5,5-tetramethyl-Δ3-pyrroline-3-methyl Methanethiosulfonate; Toronto Research Chemicals, Canada) was attached as described in (Bleicken et al., 2010). The continuous wave EPR spectra of all spin-labeled Bax variants in water were measured at room temperature to determine the efficiency of the labeling procedure. Labeling efficiencies of the doubly-labeled and singly-labeled mutants varied from 50 to 100%, which is reflected in different modulation depths in the obtained DEER traces (data not shown).

Calcein release assays

Bax activity was tested using calcein release assays as described in (Bleicken et al., 2013). In brief, for large unilamellar vesicle (LUVs) formation, lipids were mixed in chloroform, dried to thin films and resuspended at 4 mg/ml in 80 mM calcein (Sigma-Aldrich) neutralized with NaOH, followed by repeated freezing and thawing cycles, and extrusion through a 400 nm polycarbonate

membrane. Non-encapsulated calcein was removed with PD10 columns (GE healthcare). In black-96 well plates 20 nM cBid and 100 nM Bax were mixed in buffer (140 mM $NaCl_2$, 20 mM HEPES, 1 mM EDTA, pH 7) and LUVs were added before the fluorescence measurements were started in a plate reader (Infinite M200 plate reader from TECAN; excitation: 485 nm; detected emission: 525 nm). Fluorescence increase was followed over time. Shown are the data recorded after 2 h. We confirmed that all spin-labeled Bax variants (labeling efficiency in average >80% in the dimerization domain and ≥50% in the piercing domain) retained 50-120% membrane-permeabilizing activity with respect to wild type Bax based on calcein release from LUVs (Figure 1B and Figure S1B). Due to the different labeling efficiencies at each site, it is difficult to extract the actual permeabilization efficiency for the proteins carrying both labels. However, the DEER experiments on active spin-labeled Bax were performed only on the spin labeled proteins in the membrane fraction (see Supplemental methods, SM), which minimizes the potential effect of a fraction of non-functional protein, as very likely it is unable to specifically insert into membranes.

Preparation of monomeric Bax samples for DEER

Doubly-labeled Bax variants were mixed with 40% v/v deuterated glycerol to a final protein concentration of 10-25 μM, inserted in quartz tubes with 3 mm outer diameter and snap frozen in liquid nitrogen. Tubes were stored in a -80°C freezer before the DEER measurements.

Composition of the lipid mixtures and LUV preparation

The lipid mixture mimicking the mitochondrial outer membrane composition was prepared as in (Bleicken et al., 2012; Lovell et al., 2008) with 49% egg L-α-phosphatidyl choline (PC), 27% egg L-α phosphatidyl ethanolamine (PE), 10% bovine liver L-α-phosphatidyl inositol (PI), 10% 18:1

phosphatidyl serine (PS) and 4% CL (all percentages mol/mol). Lipids were mixed in chloroform and dried under vacuum overnight. Then the lipid film was resuspended in buffer (150 mM $NaCl_2$, 20 mM TRIS, pH 7.5) by extensive mixing and five cycles of freezing and thawing. Afterwards, the lipid solution was extruded 21 times through a 400 nm membrane to produce LUVs (large unilamellar vesicles).

Bax insertion into LUVs

Doubly labeled Bax (3-4 µM mixed with 10-15 µM unlabeled WT Bax; final concentrations) or singly labeled Bax (5-10 µM) was incubated for 2 minutes on ice with cBid (1-2 µM). Freshly prepared LUVs were added to the solution (final concentrations: ~10 mM lipids in a total volume of 250-400 µl) and the suspension was incubated for 1 h at 37°C. The mixture was spinned down for 30 min at 120000 g to pellet the LUVs. The pellet was separated from the supernatant and resuspended with 20 µl buffer (150 mM $NaCl_2$, 20 mM TRIS, pH 7.5). In this way the spin-labeled Bax variants were concentrated 5-10 fold. 10% v/v deuterated glycerol was added to the sample as cryoprotectant. The sample was inserted into a quartz tube with 3 mm outer diameter and snap frozen in liquid nitrogen. Tubes were stored in a -80°C freezer before the DEER measurements.

Bax activation by detergent addition

As control, selected samples were also prepared in detergent. The detergent was added to singly-labeled Bax or doubly-labeled Bax (previously diluted 1:4 with unlabeled wild type Bax) and the samples were incubated 30 min at room temperature (final concentration: 10-25 µM Bax). Afterwards 10% v/v deuterated glycerol was added as cryoprotectant, the sample was inserted into a quartz tube with 3 mm outer diameter and snap frozen in liquid nitrogen. The detergents used

were: 2% w/v DDM (n-Dodecyl-β-D-maltoside, Sigma-Aldrich) and 0.2-2% w/v OG (n-Octyl-β-D-glucopyranoside, Sigma-Aldrich).

In-organelle EPR: spin-labeled Bax in mitochondria

Singly labeled Bax (5-10 μM) was incubated for 2 minutes on ice with cBid (1-2 μM). Liver mitochondria were prepared according to (Bleicken et al., 2012). Briefly, they were isolated from albino Wistar rats (150-180 g) by differential centrifugation from the liver following (Johnson and Lardy, 1967). The liver was quickly removed and was homogenized in a Potter-Evelhjem homogenizer with isolation medium containing 250 mM sucrose, 1 mM Tris-HCl, pH 7.4 at 4°C. The homogenate was centrifuged at 1100 x g for 10 min and the resulting supernatant was centrifuged at 5000 x g for 10 min. The obtained pellet was washed by resuspending in the same buffer, and centrifuged at 12520 x g for 10 min to obtain the mitochondrial pellet. Mitochondrial protein was assayed by the Biuret method. Quantitative phosphorus analysis to obtain the lipid content was performed according to (Nakamura, 1952). The lipid concentration was determined to be 40 mg/ml. Freshly prepared mitochondria were added to the Bax-cBid solution (final concentrations: ~10 mM lipids in a total volume of 250-400 μl) and the suspension was incubated for 1 h at 37°C. The mixture was spinned down for 30 min at 120000 g to pellet the mitochondria. The pellet was separated from the supernatant and resuspended with 20 μl buffer (150 mM $NaCl_2$, 20 mM TRIS, pH 7.5). In this way the spin-labeled Bax variants were concentrated 5-10 fold. 10% v/v deuterated glycerol was added to the sample as cryoprotectant. The sample was inserted into a quartz tube with 3 mm outer diameter and snap frozen in liquid nitrogen. Tubes were stored in a -80°C freezer before the DEER measurements.

DEER measurements

DEER measurements were performed on a home-built or commercial (Bruker ELEXSYS-II E580) Q-band spectrometer (34-35 GHz) equipped with a TWT amplifier (150-200 W) and a home-made rectangular resonator enabling the insertion of 30-40 µL of sample in quartz tubes with 3 mm outer diameter (Polyhach et al., 2012; Tschaggelar et al., 2009). Dipolar time evolution data were acquired using the four-pulse DEER experiment at 50 K. All pulses were set to 12 ns with the pump frequency set at the maximum of the echo-detected field swept spectrum, 100 MHz higher than the observer frequency. Deuterium nuclear modulations were averaged by increasing the first interpulse delay by 16 ns for 8 steps (for a detailed description of the setup see (Polyhach et al., 2012)).

The background of the normalized DEER primary data (V(t)/V(0)) was fitted and the resulting normalized secondary data (F(t)/F(0)) were converted by model-free Tikhonov regularization to distance distributions with the software DeerAnalysis2013 (Jeschke et al., 2006). The simulation of the possible spin label rotamers populated at selected positions in the protein was performed using the Matlab program package MMM2013.2 based on a rotamer library approach (Polyhach et al., 2011).

Spin dilution methods to minimize inter-monomer distance

The dilution rate of spin-labeled Bax vs. unlabeled WT Bax of 1:4 was chosen after performing test experiments and making theoretical considerations (see Fig. S3). Our labeling efficiency for the Bax mutants was in average >80% in the dimerization domain and ≥50% in the piercing

domain, therefore the actual spin dilution was in fact bigger than 1:4. In general, at Q band, the DEER modulation depth for a two spin system is 0.4 for a 100% labeling efficiency. After spin dilution, we have 20% spin-labeled and 80% unlabeled protein (1:4 ratio), therefore, the spin label observed in the DEER experiment will have 20% probability to find a spin-labeled nearest neighbor. The DEER modulation depth will be only 0.2*0.4=0.08, namely 5 times less than in the undiluted case (see for example (Bode et al., 2007; von Hagens et al., 2013)). This was tested and the results are presented in Figure S3. Of course, the exact ratio between the intra-monomer (AB distance) and inter-monomer peaks (AA, BB, AB', A'B) will vary slightly for each used mutant depending on the concrete labeling efficiency of each site. This is why in order to obtain a more consistent description of the intra-monomeric distance peaks in those EPR spectra with a more complicated peak assignment we measured several samples not only in liposomes, but also in detergent (which minimizes heterogeneity in the active Bax oligomers). Finally, the residual distance peaks were always compared to the expected values based on independent measurements with the corresponding singly-labeled mutants (see for example Figure S4).

However, as not all mutants were 100% labeled or 100% active the real spin dilution factor was even bigger than 1:4. Additionally, experimental effects like differences in insertion rate or efficiency, or in the affinity between the different labeled and non-labeled Bax molecules, could also play a role in the actual probability of having two labeled Bax molecules next to each other. These effects are expected to be minimal because the mutants used in this study retained membrane permeabilization activity and we analyzed only the membrane-bound fraction. A rigorous experimental analysis of selected distance data from double-labeled mutants was also performed in order to empirically check that the use of a 1:4 dilution was appropriate.

Peak annotation process

In order to avoid artifacts, it was crucial to perform a careful peak annotation process that allowed us to distinguish desired intra-monomer distance peaks from the undesired residual inter-monomer distances arising from the presence of other labeled Bax molecules in the oligomer. The spin dilution strategy was successful (see Figure S3A-C for two examples). We used information gained from singly labeled proteins (Fig. 2G) to distinguish the intra-monomeric distances from other peaks (examples in Figure S4). Because of the fast nitroxide transverse relaxation, the length of DEER traces in membranes is limited. To compensate for this, we performed additional experiments in detergent that validated the 5-6 nm distances peaks detected in MOM LUVs (Figure S4). Notably, under the chosen conditions the distance distributions in detergent were similar to those obtained in liposomes, but the more homogeneously dispersed sample minimized the background uncertainties in DEER analysis.

Modeling of Bax using the DEER constraints

Spin label positions in the unknown *piercing* domain of Bax were localized by multilateration from reference points in the dimerization domain and determination of a probability density distribution. Its application to spin-labeled proteins is available in the freely available open-source software used here (MMM2013.2), and similar approaches were previously described (see for example Gaffney et al. 2012; Yang et al., 2012). Point localization without uncertainty isosurface is also available in another free open-source EPR software (Hagelueken et al. 2013). The reference points correspond to the mean spin label positions at labeling sites in the known part of the structure computed from a rotamer distribution, which was in turn simulated with MMM2013.2 (Polyhach et al., 2011). A first guess for the coordinates of the label in the unknown part of the

structure was obtained from a linearized form of the multilateration problem (Murphy, 2007). Briefly, with given Cartesian coordinates (x_i, y_i, z_i) of the n reference points and distances r_i of the point to be localized from the reference, we compute an n-1-by-3 matrix **A** with rows given by (x_i, y_i, z_i) - (x_1, y_1, z_1) for $i = 2\ldots n$ and a vector $\boldsymbol{b}$ with elements $\frac{1}{2}(r_i^2 - r_1^2 + d_{i1}^2)$ for ($i = 2\ldots n$). Here the d_{i1} are the distances of the i^{th} reference point from the first reference point. The solution $\boldsymbol{x}$ of the equation $\mathbf{A}\boldsymbol{x} = \boldsymbol{b}$ is computed by matrix inversion, or, if the matrix $\boldsymbol{A}$ is singular, by using the pseudo-inverse.

The first guess for the coordinates of the point to be localized is then $\boldsymbol{x}$ + (x_1, y_1, z_1). This guess is then refined by non-linear least squares minimization using a simplex algorithm.

The coordinates thus obtained define the center of a cube with 6 nm side length in which the location probability density was computed. For this the cube was sampled by a grid with uniform spacing of 0.4 Å along all three Cartesian coordinates. From the n experimental distances to the reference points and the corresponding distances of a grid point to the reference points probability densities p_i ($i = 1...\ n$) were computed for the spin label to be localized at this grid point. Gaussian distributions of the individual distances were assumed and correlations between the distributions to different reference points were neglected. The total probability density is thus the product of the n individual probability densities.

A level of the normalized probability density was determined so that a probability density isosurface at this level includes 50% of the total probability for finding the spin label. This level is the same as used in thermal ellipsoid representations of crystal structures. The isosurface was displayed as a semitransparent surface.

The algorithm is implemented in the open-source Matlab-based modeling software MMM2013.2.

Structure modeling

To create the loop section for residues 127-129, backbone dihedral angles ϕ_i and ψ_i were randomly varied in a Monte Carlo approach. The statistical distribution of these angles was taken from the residue-specific Ramachandran plots by Hovmöller *et al.* (Hovmoller et al., 2002). For the preproline residue 129V only dihedral angle pairs were accepted that fell in the allowed region of the corresponding Ramachandran plot by Lovell *et al.* (Lovell et al., 2003). In both cases, the plots were copied as bitmaps from PDF files and digitized with home-written image-processing Matlab software.

Backbone N, Cα, and carbonyl C coordinates were computed from the ϕ_i and ψ_i using the Sugeta-Miyazawa algorithm (Sugeta and Miyazawa, 1967) and standard peptide bond lengths and angles. Carbonyl O atoms were added in the peptide plane, assuming a standard bond length and standard bond angles. The initial rotation matrix **A** was computed according to (Shimanouchi, 1955) from the backbone coordinates of residue 126. Side groups were added with SCWRL4 (Krivov et al., 2009).

Models were rejected if they featured self-clashes, clashes between the model and its symmetry-related copy in the dimer, or clashes with atoms in the dimerization domain. Clashes were defined as an approach of two heavy atoms of non-consecutive residues closer than 2.7 Å.

Spin label coordinates were predicted by transforming the mean NO midpoint coordinate in a rotamer library of an unrestricted MTSL side chain (Polyhach et al., 2011) from the peptide standard frame to the local residue frame of the label site. Models were accepted if the predicted spin label's coordinate corresponded to a relative probability density of at least 0.5, normalized to the maximum probability density in the localization of the spin label localization at position 149.

All programs were implemented as subroutines of MMM2013.2 (Polyhach et al., 2011) and are available from the authors on request. A generalized loop modeler based on this approach will be implemented in a future release of the program. MMM2013.2 was also used for visualization of the models.

Cross-link experiments

Three different Bax mutants were used to cross-link the dimerization domain, the piercing domain or both: Bax C55-C87, Bax C186 and Bax C55-C87-C186, respectively. Two maleimide-based cross-linkers were used: BMH (1,6-Bismaleimidohexane, 1.3 nm distance) and BM(PEG)3 (Bis-Maleimide-PEG_3; 1.78 nn distance) (both from Thermo scientific). For each Bax variant a 100 µl reaction mix was prepared containing lipids (2 mM mitochondrial mix used for the preparation of LUVs), cBid (0.5 µM) and Bax (6.5 µM) and incubated for 45 min at 37°C. Afterwards 20 µl of the mix were incubated for 5 min at 95°C with SDS loading buffer. The residual 80 µl were separated into two equal fractions and each fraction was mixed with one of the two cross-linkers (stock solution in DMSO; final DMSO concentration in the sample <1%; cross linker 5x excess over Bax concentration) and incubated 45 min at RT. Afterwards, each mixture was incubated for 5 min at 95°C with SDS loading buffer and the samples were loaded on a Gradient SDS-PAGE (Nu-PAGE, Invitrogen).

In-cell experiments

HeLa cells were maintained in Dulbecco's modified Eagle's medium (DMEM) supplemented with 10% heat-inactivated Fetal Calf Serum (FCS) (Invitrogen) and 1% penicillin/streptomycin in 5% CO_2 at 37°C. Cells were seeded and transfected with Lipofectamine 2000 (Invitrogen) typically

with 100 ng of GFP-Bax or GFP-Bax 1-2/L-6 constructs (experiments shown in Fig. 5C) or 100 ng of GFP-Bax mutants and 100 nM pDS-Red-Mito (Clontech, experiments shown in Fig. 1C) according to the manufacturer´s instructions. Cells were maintained at 37°C and 5% CO_2 on DMEM without phenol red supplemented with FCS and containing 1 µM Staurosporine for apoptosis induction. The localization experiments in Fig. 1C were done with fixed cells (4% paraformaldehyde) while the experiments in Fig. 5C were done with live cells (stained with 100 nM TMRE (Sigma) for 20 minutes before imaging). Experiments were performed on a Zeiss LSM 710 microscope using a 40x/1.20 C-Apochromat objective (living cells) or a 63x/1.40 Apochromat (fixed cells). Images on living cells were captured over 2 h at 2 min intervals and analyzed using Fiji.

Supplemental methods: Accuracy of the DEER-NMR-X-ray approach for the model of active Bax at the membrane

To assess the significance of the combined DEER-MMM-NMR-X-ray approach which led to the model of Bax at the membrane we performed a statistical analysis based on two methods: 1. the mean square deviation between the simulated and experimental mean distances; and 2. the deviation between the localization of a spin-labeled site via multilateration and via simulation on the available structure. To show the principle of the multilateration approach available in MMM2013.2 we also provide an *in silico* example on the 1.7 Ă resolution structure of T4-lysozyme (paragraph 2.4 and Fig. S5E).

1. *Mean-distance method*

For the *mean-distance method*, we use all available experimental constraints and compare them with the corresponding distances simulated on the NMR or X-ray structures. The *rmsd* obtained is compared to the $rmsd_{DEER}$ of 3.5 Ă available in literature, based on studies on spin-labeled sites in helical regions in proteins (Jeschke, 2013). We define a "good agreement" between experimental and available structural data if the experimental *rmsd* is within $2 \cdot rmsd_{DEER}$.

1.1 Statistical Analysis on water soluble Bax: the DEER-NMR comparison: The experimental distances obtained by DEER on water soluble Bax at 50 K with 50% v/v deuterated glycerol as cryoprotectant are shown in Fig. S1E together with those simulated on the model #8 (PDB 1F16 (Suzuki et al., 2000)). The deviations δ_{jn} between exp. and simulated (sim.) mean distances are also presented in Figure S1E. The overall root mean square deviation is then calculated as:

$$rmsd_{DEER-Baxmon} = \sqrt{\frac{1}{25}\sum_{n=1}^{25}(\delta_{jn})^2} = 3.16\ \text{Ă} \qquad \text{(eq. 1)}$$

The validation performed on 25 pairs of spin-labeled sites in monomeric Bax in water showed an $rmsd_{DEER\text{-}Baxmon}$ of 3.16 Å ($0.9 \cdot rmsd_{DEER}$), which allows us to define a "very good agreement" between the DEER distances obtained in the water soluble Bax and the NMR model #8.

1.2 Statistical Analysis on membrane-embedded Bax: the DEER-X-ray comparison: The same type of analysis is performed using as template the X-ray structure of the dimerization domain (PDB 4BDU) extended to site 126. The deviations δ_{jn} between exp. and simulated (sim.) mean distances are presented in Figure S2E. The overall room mean square deviation is then calculated as:

$$rmsd_{DEER-Baxdim} = \sqrt{\frac{1}{17}\sum_{n=1}^{17}(\delta_{jn})^2} = 4.01\ \text{Ă} \qquad \text{(eq. 2)}$$

The validation performed on 17 pairs of spin-labeled sites showed an $rmsd_{DEER\text{-}Baxdim}$ of about $1.1 \cdot rmsd_{DEER}$, which allows us to define a "very good agreement" between the DEER distances obtained in the membrane-embedded dimerization domain of Bax and the X-ray structure.

1.3 Summary: The accuracy of the DEER data with respect to the available structural data are summarized in Table S1.

$rmsd_{DEER}$ (Jeschke, 2013)	$rmsd_{DEER\text{-}Bax}$	$rmsd_{DEER\text{-}Bax}/rmsd_{DEER}$	*agreement*
3.5 Ă	3.16 Ă (monomer)	0.9	Very good
	4.01 Ă (dimer)	1.1	Very good

Table S1. Accuracy of the DEER-structure comparison obtained via the mean-distance method.

2. *The multilateration method*

For the multilateration method we chose 6 specific sites in Bax, namely 55, 62, 87, 101, 126, 149. For each site more than 3 experimental constraints to other positions in the protein exist. It is worth noting that in Bax a large number of high quality DEER constraints between spin-labeled pairs within a restricted set of positions exists. The multilateration method will be applied to compare the experimental DEER data with 20 NMR structures (PDB 1F16: water soluble Bax) and with one X-ray structure (PDB 4BDU: truncated Bax dimerization domain).

2.1 Definition of uncertainties in the location of spin-labeled sites in proteins: For the multilateration method in the comparison DEER-NMR, we need to define an overall root mean square uncertainty of the NO midpoint for a given residue using the software MMM2013.2 and the 20 available NMR models ($rmsd_{NO\text{-}Baxmon}$). Then, with the experimental Bax constraints and the software MMM2013.2 we locate the chosen sites via multilateration methods on the NMR model 8 (the best model chosen based on the comparison of exp. and sim. time domain DEER data). The comparison between the errors in localizing a spin label in the best NMR structure using multilateration methods and DEER data ($rmsd_{multilat}$) and the overall root mean square displacement of the NO midpoint based on the rotamer library precision and the NMR ensemble ($rmsd_{NO\text{-}Baxmon}$) provides a consistency check for the modeling approach as well as an estimate of uncertainty of the model.

First we calculated with MMM2013.2 the MTSL rotamers at the 6 specific sites on the 20 NMR models of monomeric Bax (PDB 1F16). The mean location of the NO midpoint was obtained for

each site (*j*) for each NMR structure (*n*). The mean location of the *j-th* NO midpoint was calculated as:

$$\left(x_{j0}, y_{j0}, z_{j0}\right) = \left(\frac{1}{20}\sum_{n=1}^{20}(x_{jn}), \frac{1}{20}\sum_{n=1}^{20}(y_{jn}), \frac{1}{20}\sum_{n=1}^{20}(z_{jn})\right) \quad \text{(eq. 3)}$$

The root mean square deviation δ_{jn} of the NO midpoint for each spin-labeled site *j* in the *n-th* structure in the NMR ensemble was calculated as:

$$\delta_{jn} = \sqrt{\left(x_{jn} - x_{j0}\right)^2 + \left(y_{jn} - y_{j0}\right)^2 + \left(z_{jn} - z_{j0}\right)^2} \quad \text{(eq. 4)}$$

The overall room mean square deviation for each site *j* was then calculated as:

$$\sigma_j = \sqrt{\frac{1}{20}\sum_{n=1}^{20}(\delta_{jn})^2} \quad \text{(eq. 5)}$$

The results are summarized in Table S2.

***j-th* site in Bax**	**σ_j [Å]**	**$(\sigma_j)^2$ [Å^2]**
55	2.06	4.24
62	2.76	7.62
87	2.60	6.76
101	3.36	11.29
126	1.66	2.76
149	2.23	4.97

Table S2. Root mean square deviations in the position of the nitroxide midpoint in the 20 NMR models of monomeric Bax (PDB 1F16).

Based on the 6 available sites, the average root mean square displacement of the NO midpoint obtained by MMM2013.2 on the 20 NMR models of the PDB file 1F16 is:

$$rmsd_{NMR} = \sqrt{\frac{1}{6}\sum_{j=1}^{6}(\sigma_j)^2} = 2.5 \text{ Å} \qquad \text{(eq. 6)}$$

This $rmsd_{NMR}$ is based on the variability in the specific NMR ensemble under investigation and on the position of the chosen site (e.g. helical vs. loop positions), calculated with the MMM approach (MTSL library in MMM2013.2). If we now additionally take into account the average $rmsd_{DEER}$ of 3.5 Ă between simulated and experimental distances based on a number of available data mainly in helical positions (Jeschke, 2013), resulting in an $rmsd_{DEER\_site}$ of 2.47 Ă, we obtain the overall expected root mean square error of the NO midpoint position on the monomeric structure of Bax (PDB 1F16) using MMM2013.2:

$$rmsd_{NO-Baxmon} = \sqrt{(rmsd_{NMR})^2 + \frac{(rmsd_{DEER})^2}{2}} = 3.5 \text{ Å} \qquad \text{(eq. 7)}$$

This is our reference *rmsd* to obtain the accuracy of the DEER data with respect to the NMR structure of water soluble Bax. In fact we will consider an experimental $rmsd_{multilat}$ within $2 \cdot rmsd_{NO\text{-}Bax}$ as a good agreement between experimental distances and structural data.

For the multilateration method in the comparison DEER-X-ray, we have a unique set of coordinates in the 3 Ă resolution X-ray structure of the truncated dimer in detergent (PDB 4BDU). To obtain an $rmsd_{X\text{-}ray}$, analogous to the $rmsd_{NMR}$ (eq. 6) we can either consider the X-ray resolution (*RES.*) as an estimate for the $rmsd_{X\text{-}ray}$ and in this case we would obtain:

$$rmsd^{RES}{}_{NO-Baxdim} = \sqrt{\left(RES._{X-ray}\right)^2 + \frac{(rmsd_{DEER})^2}{2}} = \sqrt{(3.0)^2 + \frac{(3.5)^2}{2}} = 3.99 \text{ Å} \quad \text{(eq. 8)}$$

or analyze the Debye-Waller or temperature factors (B-factors) of the residues of Bax in the crystal, which give information on local structural flexibility, thermal stability, and heterogeneity of the macromolecule. We used the root mean-square fluctuations (*rmsf*) which can be obtained through B-factors in X-ray experiments using the following equation:

$$rmsf_i^{\,2} = \frac{3B_i}{8\pi^2} \qquad \text{(eq. 9)}$$

where B-factors are usually defined as a measure of spatial fluctuations of atoms around their average position and where their motion is described as an isotropic Gaussian distribution of displacements about the average position. We use the relation described by Kuzmanic et al. (Kuzmanic and Zagrovic, 2010) to calculate the $rmsd_{X\text{-}ray}$ using residues 54-119 of chains A and B in the dimerization domain elongated to site 126, which was used for the modeling (in total 1050 atoms):

$$rmsd_{X-ray} = \sqrt{\langle rmsd_{X-ray}{}^2 \rangle} \approx \sqrt{\frac{2}{1050}\sum_i^{1050}\frac{3B_i}{8\pi^2}} = 2.0 \text{ Å} \qquad \text{(eq. 10)}$$

By using this as a reference value for the $rmsd_{X\text{-}ray}$ we obtain:

$$rmsd_{NO-Baxdim} = \sqrt{(rmsd_{X-ray})^2 + \frac{(rmsd_{DEER})^2}{2}} = \sqrt{(2.0)^2 + \frac{(3.5)^2}{2}} = 3.2 \text{ Å} \qquad \text{(eq. 11)}$$

In the case of active Bax at the membrane, in analogy to what we described before for the case of water soluble Bax, we will consider an $rmsd_{multilat}$ within $2 \cdot rmsd_{NO\text{-}Baxdim}$ as a good agreement between the structure of the dimerization domain and the DEER data.

2.2 Statistical Analysis on water soluble Bax: the DEER-NMR comparison: The multilateration method locates 6 spin-labeled sites (55, 62, 87, 101, 126, 149) on the chosen NMR model #8 using all available experimental distance constraints to other spin-labeled residues. The resulting

$rmsd_{multilat}$ between the predicted location of the NO midpoint with highest probability (via multilateration method) and the mean NO midpoint position obtained by MMM2013.2 on the same model 8 is calculated. First we obtained the displacement between the localized NO midpoint and the one simulated on model #8 with MMM2013.2.

***j-th* site in Bax**	***Displacement with respect to MMM calculation on model #8* [Å]**	***Number of constraints to the j-th site***
55	6.3	4
62	3.2	5
87	2.9	6
101	5.4	5
126	5.2	7
149	5.4	5

Table S3. Displacement of the NO midpoint using multilateration methods and DEER data on the NMR model #8 (PDB 1F16). Two examples of localization are shown in Figure S5.

We find that all displacements ($\Delta_{multilat,j}$) fall within $2 \cdot rmsd_{NO\text{-}Baxmon}$. The overall $rmsd_{multilat}$ calculated according to eq. 12 is 4.9 Å, which is $1.4 \cdot rmsd_{NO\text{-}Bax}$ (defined in eq. 7).

$$rmsd_{multilat} = \sqrt{\frac{1}{6}\sum_{j=1}^{6}(\Delta_{tri,j})^2} = 4.9 \text{ Å} \qquad \text{(eq. 12)}$$

An $rmsd_{multilat}$ within $2 \cdot rmsd_{NO\text{-}Bax}$ is what we define a "good agreement" between the DEER distances obtained in water soluble Bax and the NMR model #8.

2.3 Statistical Analysis on membrane-embedded Bax: the DEER-X-ray comparison: To create the model of Bax at the membrane, we used the dimerization domain crystal structure (4BDU), elongated by us to position 126. To validate this dimerization domain, we used the multilateration method to localize 62, 87 and 126 based on the experimental distances.

Localization of site 126: The calculated $\Delta_{multilat,126}$ for position 126 (chain A, isosurface presented in Figure S5D), for which we have 5 DEER constraints to 55, 62, 72, 87, 101 in the chain A of the dimerization domain is 8.9 Ă. The experimental distances towards site 126 are consistent, in fact the 126-NO can be localized with 97% probability, with a mean data inconsistency of only 0.32 Ă. However it deviates by 9 Ă from that calculated by MMM2013.2 on the PDB file. By adding also the broad 126-126 constraint between chains A and B, we obtain a very similar localization (0.45 Ă inconsistency, 96.7% localization probability with a deviation of 9.2 Ă, data not shown), indicating that the A-B constraint is consistent with the set of intra-monomeric distances used. The obtained deviation of $\mathbf{2.9 \cdot} \boldsymbol{rmsd}_{NO\text{-}Baxdim}$ can be still considered a reasonable agreement between DEER data and the X-ray structure of the dimer.

We cannot however rule out that there may be a slight rearrangement of the end of helix 5, especially because this is the region where the kink appears and the two domains disengage in the active conformation. For completeness, we also took into account this displacement of site 126 to recalculate the location of 149, using the calculated location of site 126 rather than the position simulated in the helix-elongated X-ray structure. Main features of the model, namely the kink between helices 5 and 6 as well as localization of residue 149 in a plane about 40 Å below the center of gravity of the dimerization domain were confirmed.

Localization of site 62: As a second consistency check, we localize position 62 in helix 2 using 4 constraints to 87, 101, 126 (chain A in the dimerization domain) and to 62 (chain B in the dimerization domain). The geometry of the chosen constraints does not allow a good localization and the probability distribution is rather broad. However we could obtain a mean data inconsistency of 0.2 Ă, and a 99.6% location probability, which deviates by 8 Ă (**2.5·*rmsd*$_{NO\text{-}Baxdim}$**) from the mean position calculated by MMM 2013.2 at site 62.

Additionally, we re-localize position 62 in helix 2 using 5 constraints to 62 (B chain dimerization domain), 87, 101, 126 (A chain dimerization domain) and to 149 (A chain modeled piercing domain). Note that the first four constraints were not previously used for localization of 149, thus they are independent on the model proposed. The data set can be then considered a consistency check for the accuracy of the dimerization domains' arrangement with respect to the positioning of residue 149. We obtained a good localization of 62 (a mean data inconsistency of 1.59 Ă, and a 66% location probability), which deviates only by 2.2 Ă (0.7·*rmsd*$_{NO\text{-}Baxdim}$) from the mean position calculated by MMM2013.2 at site 62.

Localization of site 87: As a third consistency check, we localize position 87 using five constraints to 55, 62, 72, 126 (chain A in the dimerization domain) and to 87 (chain B in the dimerization domain). The geometry of the chosen constraints does not allow a good localization and the probability distribution is rather broad. However we could obtain a mean data inconsistency of 4.28 Ă, and a 94.6% location probability, which deviates by 5.9 Ă (**1.8·*rmsd*$_{NO\text{-}Baxdim}$**) from the mean position calculated by MMM2013.2 at site 87 (isosurface presented in Figure S5D).

Additionally, we re-localize position 87 using six constraints to 87 (B chain dimerization domain), 55, 62, 72, 126 (A chain dimerization domain) and to 149 (A chain modeled piercing domain).

Note that five out of six constraints were not previously used for the localization of 149, thus they are independent on the model proposed. The data set can be then considered a consistency check for the accuracy of the dimerization domain's arrangement with respect to the positioning of the 149. We obtained a good localization of 87 (a mean data inconsistency of 4.38 Å, and a 90% location probability), which deviates only by 5.2 Å ($1.6 \cdot rmsd_{NO\text{-}Baxdim}$) from the mean position calculated by MMM2013.2 at site 87.

For lack of constraints we cannot extend the multilateration validation to sites other than 126, 62 and 87. However, the obtained $rmsd_{multilat}$ values ($2.9 \cdot rmsd_{NO\text{-}Baxdim}$, $2.5 \cdot rmsd_{NO\text{-}Baxdim}$, $1.8 \cdot rmsd_{NO\text{-}Baxdim}$, respectively) are close to the $2 \cdot rmsd_{NO\text{-}Baxdim}$ threshold, indicating reasonable agreement between the DEER distances obtained in the membrane-embedded dimerization domain of Bax and the X-ray structure.

2.4 In silico example of the multilateration approach: To show the principle of the multilateration approach available in MMM2013.2 we provide an *in silico* example on the 1.7 Å resolution structure of T4-lysozyme (PDB 2LZM, see Fig. S5E). We calculated the localization of a spin-labeled site (position 72 in T4-lysozyme) based on *in silico* simulated distances to 5 sites labeled with MMM2013.2. The highest probability of location of 72 deviates 2.5 Å from the mean NO-midpoint of the simulated rotamers at the same site. This is the degree of intrinsic accuracy of the method using *in silico* distances in MMM2013.2 and the approximation of the mean position of the nitroxide midpoints as reference point for each site. It was not possible to validate the multilateration approach with experimental constraints towards position 72 (or other sites) in this structurally stable globular protein due to lack of experimental constraints. It is important to

highlight that the accuracy of the prediction of the spin label location based on experimental data in frozen molecular ensembles depends on the dynamic nature of the regions investigated (as in the case of helices 6-9 in Bax, see Table S4).

2.5 Summary: The accuracy of DEER with respect to the available structures is summarized in Table S4.

Reference $rmsd_{NO\text{-}Bax}$	$rmsd_{multilat}$	$rmsd_{multilat}$ /$rmsd_{NO\text{-}Bax}$	*agreement*
3.5 Å ($rmsd_{NO\text{-}Baxmon}$)	4.9 Å (monomer)	1.4	Good
3.2 Å ($rmsd_{NO\text{-}Baxdim}$)	7.8 Å (dimer)	1.9	Reasonable

Table S4. Accuracy of the DEER-structure comparison obtained via the multilateration method.

Conclusions: Overall, we could demonstrate that agreement between experimental DEER data and available atomistic structures is good to very good for the physiological native inactive structure in water (PDB 1F16) and reasonable to good for the crystallized dimeric structure obtained from detergent. This justifies using these structures as a starting point for the modeling of the piercing domain in active Bax at the membrane. Furthermore, this analysis sets an accuracy or resolution of 8 Å for the proposed structural model of Bax at the membrane.

When comparing a single X-ray structure of truncated Bax protein fused to GFPs with DEER data for full length Bax in liposomes, some of the deviation may be due to genuine differences in the structure caused by the different environment. Additionally, for a dynamic protein domain, such as the piercing domain in Bax, the concept of a single atomistic structure is inappropriate. This

means that at least part of the uncertainty of the model is unavoidable; the structural ensemble is broad. The distance distributions of the EPR constraints reflect the variability within the frozen ensemble of structures, which is clearly seen from the fact that much broader distributions are observed for site pairs involving the piercing domain than for most site pairs that are entirely in the dimerization domain. It is an advantage of the EPR technique that such disorder can be detected by measuring distance distributions rather than only mean values for the distance.

Supplemental References

Bleicken, S., Classen, M., Padmavathi, P.V., Ishikawa, T., Zeth, K., Steinhoff, H.J., and Bordignon, E. (2010). Molecular details of Bax activation, oligomerization, and membrane insertion. J Biol Chem *285*, 6636-6647.

Bleicken, S., Garcia-Saez, A.J., Conte, E., and Bordignon, E. (2012). Dynamic interaction of cBid with detergents, liposomes and mitochondria. PLoS One *7*, e35910.

Bleicken, S., Wagner, C., and García-Sáez, Ana J. (2013). Mechanistic Differences in the Membrane Activity of Bax and Bcl-xL Correlate with Their Opposing Roles in Apoptosis. Biophys J *104*, 421-431.

Bode, B.E., Margraf, D., Plackmeyer, J., Dürner, G., Prisner, T.F., and Schiemann, O. (2007). Counting the Monomers in Nanometer-Sized Oligomers by Pulsed Electron−Electron Double Resonance. J Am Chem Soc *129*, 6736-6745.

Chong, S., Mersha, F.B., Comb, D.G., Scott, M.E., Landry, D., Vence, L.M., Perler, F.B., Benner, J., Kucera, R.B., Hirvonen, C.A.*, et al.* (1997). Single-column purification of free recombinant proteins using a self-cleavable affinity tag derived from a protein splicing element. Gene *192*, 271-281.

Czabotar, Peter E., Westphal, D., Dewson, G., Ma, S., Hockings, C., Fairlie, W.D., Lee, Erinna F., Yao, S., Robin, Adeline Y., Smith, Brian J.*, et al.* (2013). Bax Crystal Structures Reveal How BH3 Domains Activate Bax and Nucleate Its Oligomerization to Induce Apoptosis. Cell *152*, 519-531.

Desagher, S., Osen-Sand, A., Nichols, A., Eskes, R., Montessuit, S., Lauper, S., Maundrell, K., Antonsson, B., and Martinou, J.C. (1999). Bid-induced conformational change of Bax is responsible for mitochondrial cytochrome c release during apoptosis. J Cell Biol *144*, 891-901.

Dewson, G., Ma, S., Frederick, P., Hockings, C., Tan, I., Kratina, T., and Kluck, R.M. (2012). Bax dimerizes via a symmetric BH3:groove interface during apoptosis. Cell Death Differ *19*, 661-670.

Gaffney, B.J., Bradshaw, M.D., Frausto, S.D., Wu, F., Freed, J.H., and Borbat, P. (2012). Locating a lipid at the portal to the lipoxygenase active site. Biophys J 103, 2134-2144.

Hagelueken G., Abdullin D., Ward R., Schiemann O. (2013). mtsslSuite: In silico spin labelling, trilateration and distance-constrained rigid body docking in PyMOL. Mol Phys *111*(18-19), 2757-2766.

Hovmoller, S., Zhou, T., and Ohlson, T. (2002). Conformations of amino acids in proteins. Acta Crystallogr D Biol Crystallogr *58*, 768-776.

Jeschke, G. (2013). Conformational dynamics and distribution of nitroxide spin labels. Prog Nucl Magn Reson Spectrosc *72*, 42-60.

Jeschke, G., Chechik, V., Ionita, P., Godt, A., Zimmermann, H., Banham, J., Timmel, C.R., Hilger, D., and Jung, H. (2006). DeerAnalysis2006—a comprehensive software package for analyzing pulsed ELDOR data. Appl Magn Reson *30*, 473-498.

Jeschke, G., Sajid, M., Schulte, M., and Godt, A. (2009). Three-spin correlations in double electron-electron resonance. Phys Chem Chem Phys *11*, 6580-6591.

Johnson, D., and Lardy, H. (1967). Isolation of liver or kidney mitochondria. In Methods in Enzymology, M.E.P. Ronald W. Estabrook, ed. (Academic Press), pp. 94-96.

Krivov, G.G., Shapovalov, M.V., and Dunbrack, R.L., Jr. (2009). Improved prediction of protein side-chain conformations with SCWRL4. Proteins *77*, 778-795.

Kuzmanic, A., and Zagrovic, B. (2010). Determination of ensemble-average pairwise root mean-square deviation from experimental B-factors. Biophys J *98*, 861-871.

Lovell, J.F., Billen, L.P., Bindner, S., Shamas-Din, A., Fradin, C., Leber, B., and Andrews, D.W. (2008). Membrane binding by tBid initiates an ordered series of events culminating in membrane permeabilization by Bax. Cell *135*, 1074-1084.

Lovell, S.C., Davis, I.W., Arendall, W.B., 3rd, de Bakker, P.I., Word, J.M., Prisant, M.G., Richardson, J.S., and Richardson, D.C. (2003). Structure validation by Calpha geometry: phi,psi and Cbeta deviation. Proteins *50*, 437-450.

Murphy, W. S. Jr. Determination of a position using approximate distances and trilateration. Master thesis, Department of Applied Mathematics and Statistics, Colorado School of Mines, Golden, Colorado, USA (2007).

Nakamura, G.R. (1952). Microdetermination of Phosphorus. Analytical Chemistry *24*, 1372-1372.

Polyhach, Y., Bordignon, E., and Jeschke, G. (2011). Rotamer libraries of spin labelled cysteines for protein studies. Phys Chem Chem Phys *13*, 2356-2366.

Polyhach, Y., Bordignon, E., Tschaggelar, R., Gandra, S., Godt, A., and Jeschke, G. (2012). High sensitivity and versatility of the DEER experiment on nitroxide radical pairs at Q-band frequencies. Phys Chem Chem Phys *14*, 10762-10773.

Shimanouchi, T.M., S.- I. (1955). On the Helical Configuration of a Polymer Chain. J Chem Phys *23*, 707-711.

Sugeta, H., and Miyazawa, T. (1967). General method for calculating helical parameters of polymer chains from bond lengths, bond angles, and internal-rotation angles. Biopolymers *5*, 673-679.

Suzuki, M., Youle, R.J., and Tjandra, N. (2000). Structure of Bax: coregulation of dimer formation and intracellular localization. Cell *103*, 645-654.

Tschaggelar, R., Kasumaj, B., Santangelo, M.G., Forrer, J., Leger, P., Dube, H., Diederich, F., Harmer, J., Schuhmann, R., García-Rubio, I.*, et al.* (2009). Cryogenic 35GHz pulse ENDOR probehead accommodating large sample sizes: Performance and applications. J Magn Reson *200*, 81-87.

von Hagens, T., Polyhach, Y., Sajid, M., Godt, A., and Jeschke, G. (2013). Suppression of ghost distances in multiple-spin double electron-electron resonance. Phys Chem Chem Phys *15*, 5854-5866.

Yang, Z., Kurpiewski M.R., Ji M., Townsend J.E., Mehta P., Jen-Jacobson L., Saxena S. (2012). ESR spectroscopy identifies inhibitory Cu^{2+} sites in a DNA-modifying enzyme to reveal determinants of catalytic specificity. Proc Natl Acad Sci U S A *109*(17), E993-1000